

THERMAL AND THERMOMECHANICAL TREATMENT

UDC 669.15:669.018.8:669.017.3:669.1.017:620.186-187

EFFECT OF THE RATE AND TEMPERATURE OF HOT DEFORMATION ON STRAIN RESISTANCE OF DUPLEX STAINLESS STEEL

Zhichao Li,^{1,2,3} Jing Wu,¹ Qiannan Li,¹ Xinjing Li,¹ Lianfang He,¹ Huiping Li,¹ and Zhihui Cai⁴Translated from *Metallovedenie i Termicheskaya Obrabotka Metallov*, No. 2, pp. 3 – 12, February, 2023.*Original article submitted March 11, 2022.*

The effect of the temperature and rate of hot deformation on the structure and strain resistance of duplex stainless steel DSS 2205 is considered. Tests for hot compression of specimens are conducted at a temperature of 1223 – 1473 K and deformation rate 0.01 – 30 sec⁻¹ to a degree of 0.4 and 0.8. Maps of deformation mechanisms are plotted. It is shown that the strain resistance decreases after attaining a maximum value in the flow curve, and the flow stress increases with decrease of the temperature and increase of the rate of the deformation. The activation energy of the hot deformation is shown to vary in accordance with the partitioning of strain between the two phases (ferrite and austenite) in the structure of the steel. The rate and the temperature of the deformation affect the deformability of the duplex steel considerably. Continuous dynamic recrystallization of ferrite is activated strongly in the range of flow stability. The range of flow instability is characterized by weak continuous dynamic recrystallization in the ferrite and discontinuous dynamic recrystallization in the austenite.

Key words: duplex stainless steel, hot deformation, strain rate, deformation temperature, flow stability, microstructure.

INTRODUCTION

Duplex stainless steels (DSSs) possess high stress corrosion resistance, excellent mechanical properties and good weldability, which makes them an alternative to single-phase ferritic or austenitic stainless steels [1 – 3]. As a rule, the mechanisms of hot deformation of ferrite and austenite differ substantially. In the case of ferrite, the high energy of stacking faults provides transverse slip or climb of dislocations, which improves the hot deformability of the steels. On the contrary, austenite exhibits limited dynamic retrogression

due to the low energy of stacking faults, and dynamic recrystallization does not occur until the attainment of critical strain [4 – 9]. In steels with duplex microstructure, the coexistence of two phases commonly causes strain partitioning during hot deformation. At first the deformation develops due to the soft ferrite [10]. In further hot deformation, the stress is gradually transferred into the austenite, which lowers the degree of the strain hardening of the metal and raises the dislocation density in the structure. The difference in the mechanisms of plastic flow and in the coefficients of thermal expansion of the austenite and of the ferrite lowers the hot workability of the duplex steel and results in formation of defects on the surface [11].

By the data of [12, 13], the plastic flow of each phase of a duplex microstructure under hot deformation occurs by a mechanism differing from the behavior of these phases in single-phase stainless steels. The authors of [12] assume that the high plasticity of ferrite in DSSs is provided by dynamic retrogression and continuous dynamic recrystallization. At the same time, it is shown in [13] that the plasticity of the

¹ School of Materials Science and Engineering, Shandong University of Science and Technology, Qingdao, Shandong, China (e-mail: lizc@sdust.edu.cn; lihuiping99@163.com).

² School of Materials Science and Engineering, Xiangtan University, Xiangtan, Hunan, China.

³ Mengshan Steel Structure Engineering Co., Ltd, Jining, Shandong, China.

⁴ School of Mechanical Engineering, Taiyuan University of Science and Technology, Taiyuan, Shanxi, China.

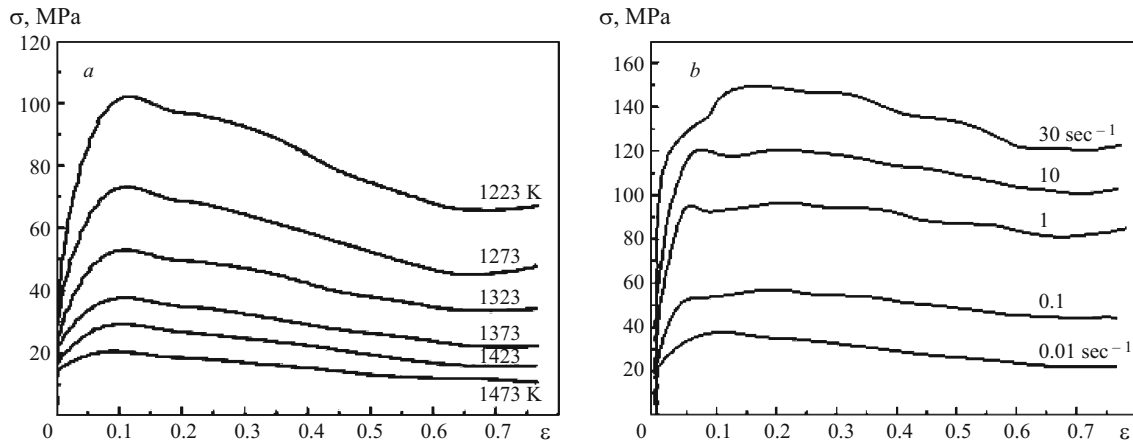


Fig. 1. Curves of plastic flow (true stress σ – true strain ϵ) for different conditions of deformation of steel DSS 2205. The figures at the curves present: a) the deformation temperature at $\dot{\epsilon} = 0.01 \text{ sec}^{-1}$; b) the deformation rate at $T = 1373 \text{ K}$.

austenite is a result of limited dynamic retrogression, and the dynamic recrystallization of the austenite is suppressed due to the presence of a soft ferritic phase. The features of plastic flow of each phase in duplex stainless steels have attracted much interest, but the effects of the process parameters (the strain rate and the deformation temperature) on the hot deformability of DSSs remain unclear.

Development of processing maps is an important approach for determining safe modes of hot processing of steels and alloys and preventing instability of the metal flow. For example, the processing maps obtained in [14] for a nickel-base superalloy have been used to determine optimum parameters of its hot treatment, i.e., the strain rate and the deformation temperature. A similar approach has been used in [15] to study the effect of the strain rate on the deformation map for superalloy 20.0Cr – 1.5Nb – 1.0Al – 2.5Ti – Ni and to determine the strain rate and the deformation temperature required for formation of a fine and homogeneous microstructure. However, fundamental studies of the hot processibility of DSSs have not been reported.

The aim of the present study was to investigate the interrelation between the parameters of hot deformation and the evolution of the microstructure of steel DSS 2205.

METHODS OF STUDY

We studied duplex stainless steel DSS 2205 (the Russian counterpart is 02Kh22N5M3) of the following chemical composition (in wt.%): 0.019 C, 23.61 Cr, 5.12 Ni, 3.36 Mo, 1.67 Mn, 0.37 Si, 0.19 N.

The ingots were hot forged into rods in the temperature range 1323 – 1423 K. The rods were quenched in water after a 300-sec hold at 1323 K. Cylindrical specimens with diameter 10 mm and length 15 mm were cut from the rods.

The tests for hot compression were conducted in a Gleeble-3500 facility. The specimens were heated to 1526 K, held for 350 sec to homogenize the chemical composition

and the microstructure of the initial steel, and then cooled at a rate of 5 K/sec to the specified temperature. Before testing for hot compression, every specimen was held at the preset temperature for 15 sec to avoid a radial temperature gradient. A thermocouple was welded in the middle of the specimen to control the actual test temperature. The strain rate during the tests was varied from 0.01 to 30 – 1 sec^{-1} , the temperature was varied from 1223 to 1473 K, the true strain $\epsilon = 0.4$ and 0.8. After the deformation, the specimens were quenched in water. The deformed specimens were cut in parallel to the deformation axis and electropolished using 90% ethanol and 10% perchloric acid for a EBSD analysis or polished electrolytically in a 6% alcoholic solution of perchloric acid for optical microscopy. The quantitative analysis of the microstructure was made using the Image Pro-Plus software.

RESULTS AND DISCUSSION

Plastic flow behavior. As a result of the tests for hot compression we obtained the true stress-strain curves (Fig. 1). The flow stress increased considerably with lowering of the temperature and elevating of the strain rate. All the deformation curves demonstrate stress lowering after the attainment of a maximum, which indicates occurrence of dynamic recrystallization during the plastic deformation. The curves have some other specific features, for example, are wavier at 1373 K at 1 – 30 sec^{-1} than at lower strain rates.

The effect of the strain rate and of the deformation temperature on the flow behavior of the metal may be described in terms of the Zener–Hollomon parameter Z [16, 17], i.e.,

$$Z = \dot{\epsilon} \exp\left(\frac{Q_p}{RT}\right), \quad (1)$$

where $\dot{\epsilon}$ is the strain rate (sec^{-1}); Q_p is the activation energy under the hot deformation, which corresponds to the peak

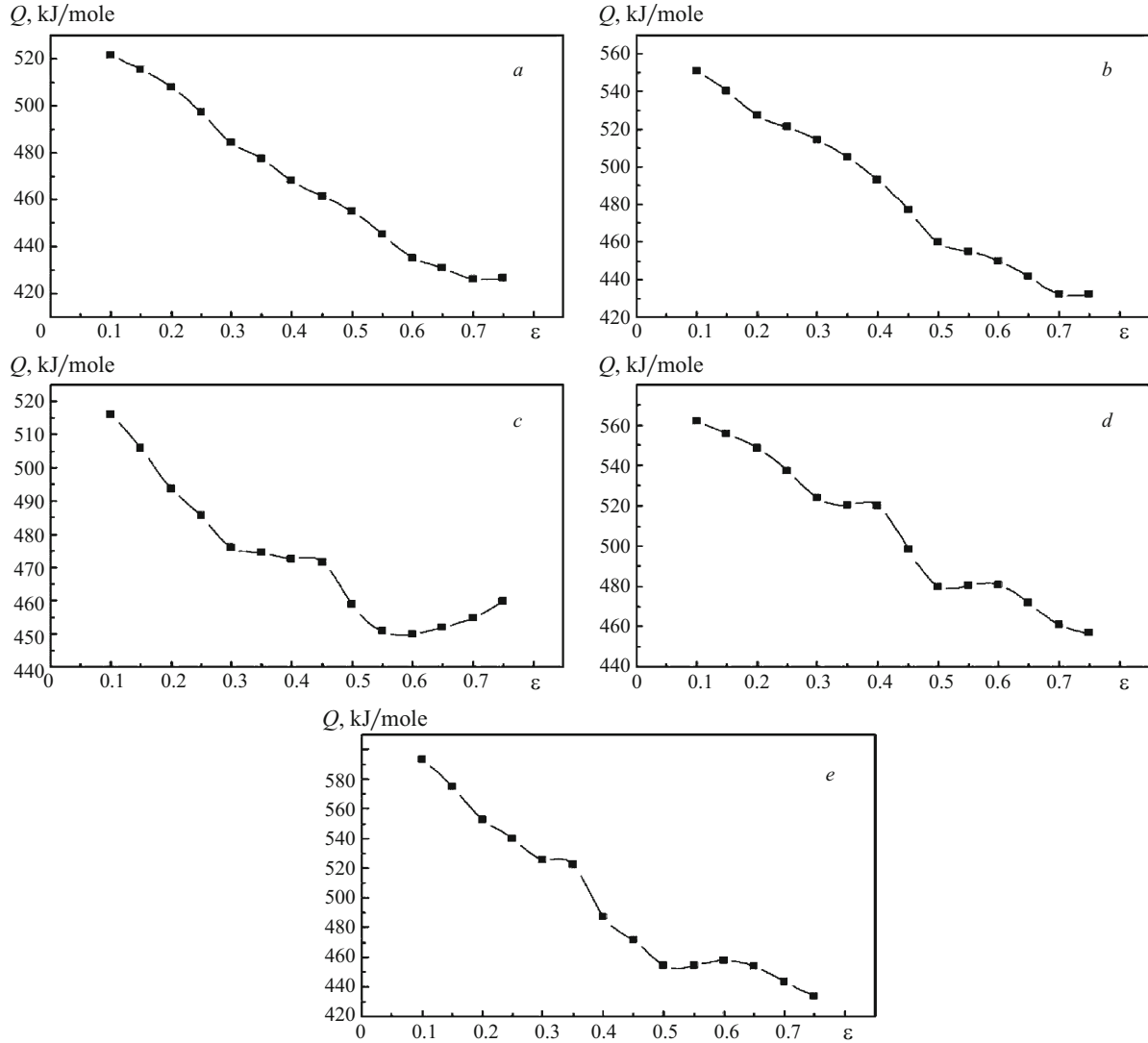


Fig. 2. Dependence of the activation energy Q of hot deformation of steel DSS 2205 on true strain ε at different strain rates: a) $\dot{\varepsilon} = 0.01 \text{ sec}^{-1}$; b) $\dot{\varepsilon} = 0.1 \text{ sec}^{-1}$; c) $\dot{\varepsilon} = 1.0 \text{ sec}^{-1}$; d) $\dot{\varepsilon} = 10 \text{ sec}^{-1}$; e) $\dot{\varepsilon} = 30 \text{ sec}^{-1}$.

stress (kJ/mole); $R = 8.314 \text{ J}/(\text{mole} \cdot \text{K})$ is the gas constant; and T is the temperature (K). It follows from Eq. (1) that the higher the strain rate and the lower the temperature, the higher the value of Z . The activation energy Q is determined from an Arrhenius-type equation [18]

$$Q = R \left(\frac{\partial \ln \dot{\varepsilon}}{\partial \ln [\sinh(\alpha\sigma)]} \right)_T \left(\frac{\partial \ln [\sinh(\alpha\sigma)]}{\partial (1/T)} \right)_{\dot{\varepsilon}}, \quad (2)$$

where α is a constant determined for the material from the relationship between σ_p , $\ln \sigma_p$ and $\ln \dot{\varepsilon}_p$. We used Eq. (2) to determine the dependences of the activation energy Q of the strain ε for different strain rates $\dot{\varepsilon}$ (Fig. 2). For all the strain rates, the value of Q decreased with growth of the strain due to the decrease of the compressive stresses. However, at a low strain rate ($\dot{\varepsilon} = 0.01$ and 0.1 sec^{-1}) Q decreases monotonically with growth of ε from 0.10 to 0.75; at a higher

strain rate ($\dot{\varepsilon} = 1, 10$ and 30 sec^{-1}) the decrease is interrupted and exhibits a step in the middle (or intermediate) deformation stage.

By the data of earlier studies [13, 19] increase of the strain rate improves the characteristics of plastic deformation of austenite in duplex stainless steels. In the case of a duplex microstructure in the DSS, the coexistence of a soft ferritic and hard austenitic phases often causes strain partitioning in the early stages of the deformation, when the strain is mostly accommodated by the softer ferrite [10]. With increase of the degree of compression, the strain transfers gradually from the ferrite phase to the austenite one, which results in accumulation of the strain energy in the later deformation stages. It can be seen from Fig. 2c – e that the values of Q do not virtually decrease in the intermediate deformation stage, when the strain grows due to the simultaneous action of the mechanisms of relaxation in the ferrite and of strain hardening in the austenite. However, if the strain parameters are favorable

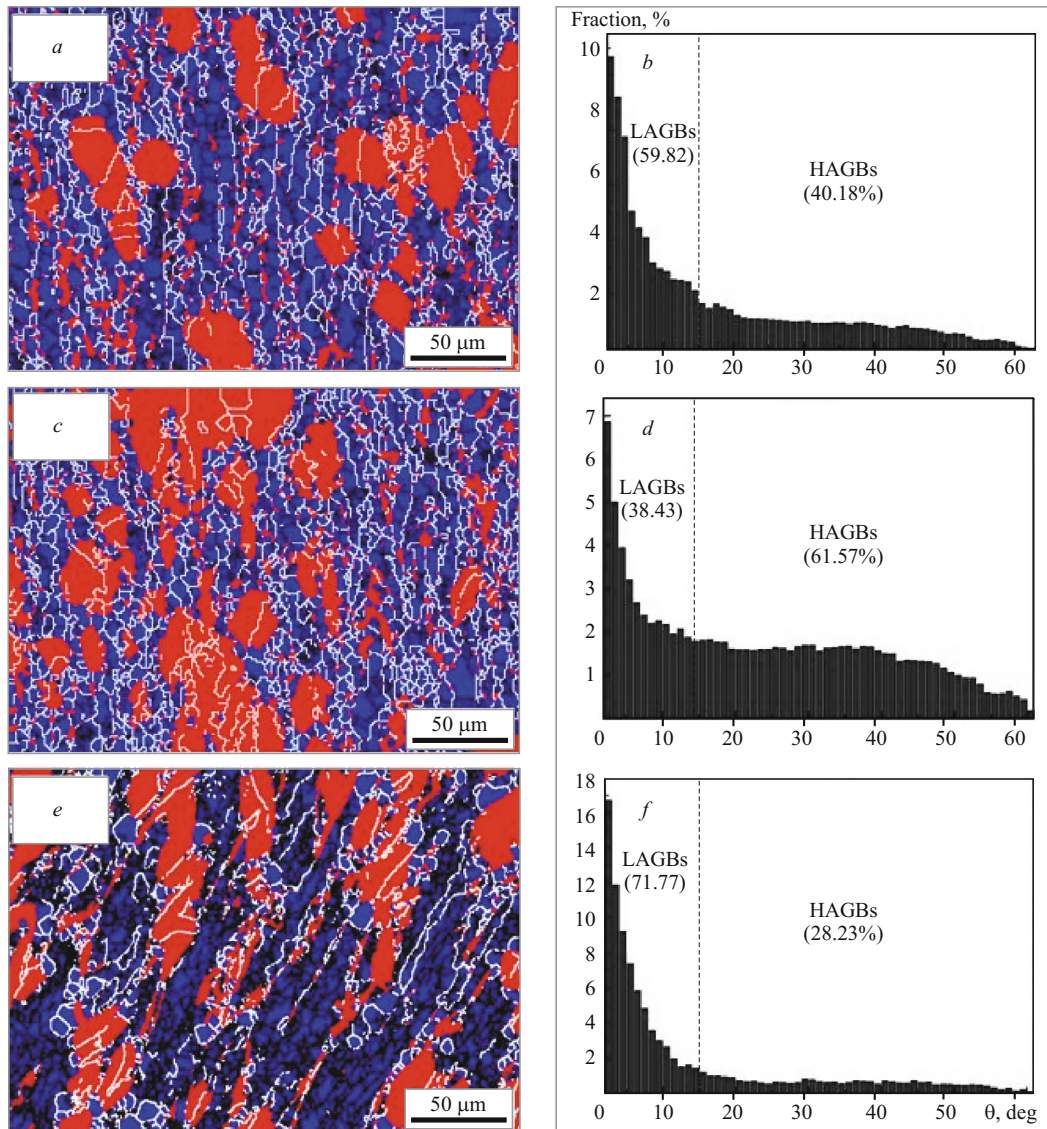


Fig. 3. EBSD maps of misorientations of ferrite and austenite grains (*a, c, e*) and the respective histograms of distribution of grain boundaries in ferrite with respect to misorientation angles θ (*b, d, f*) for different deformation parameters of steel DSS 2205 (part I): *a, b*) $T = 1323$ K, $\dot{\epsilon} = 0.01 \text{ sec}^{-1}$, $\epsilon = 0.4$; *c, d*) $T = 1323$ K, $\dot{\epsilon} = 0.01 \text{ sec}^{-1}$, $\epsilon = 0.8$; *e, f*) $T = 1323$ K, $\dot{\epsilon} = 30 \text{ sec}^{-1}$, $\epsilon = 0.8$; LAGBs and HAGBs are the low-angle and high-angle grain boundaries, respectively.

for occurrence of dynamic retrogression in ferrite (at a lower strain rate), the stress in the ferrite is kept at a relatively low level, which hinders the transfer of strain into the austenite. In this case, the deformation of ferrite is a dominant factor, and this determines the continuous (without a step) lowering of Q at $\epsilon = 0.1 - 0.75$.

Evolution of microstructure. Figure 3 presents the EBSD maps of the misorientations of ferrite and austenite grains and the respective histograms of the distribution of grain boundaries in the ferrite with respect to the misorientation angles for different deformation parameters. The blue and red colors in the EBSD images are used to depict the ferrite and austenite phases, respectively. The black lines depict

the low-angle grain boundaries (LAGB, $\theta \leq 15^\circ$); the white lines depict the high-angle grain boundaries (HAGB, $\theta \geq 15^\circ$).

When the compression is implemented at a relatively low strain rate (0.01 sec^{-1}) at 1323 K (Fig. 3*a* and *b*), the ferrite exhibits numerous LAGB with misorientation angle $\theta \leq 15^\circ$ after the true strain 0.4. This indicates occurrence of dynamic retrogression due to annihilation and redistribution of the strain-induced dislocations. The austenite in the microstructure remains virtually undeformed. When the true strain increases from 0.4 to 0.8 (Fig. 3*c* and *d*), the proportion of HAGB in the ferrite increases considerably (from about 40% to about 62%). It may be inferred that many dislocations aris-

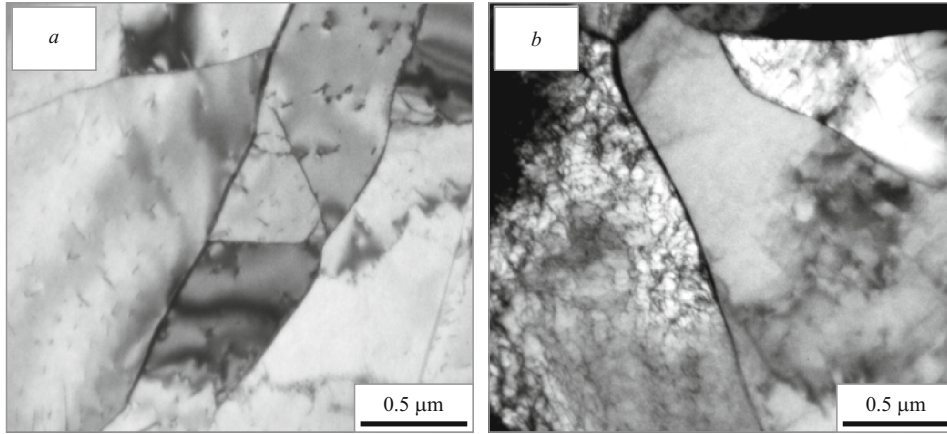


Fig. 4. Microstructure of steel DSS 2205 (TEM) after true deformation $\varepsilon = 0.4$ at 1323 K at a rate $\dot{\varepsilon} = 0.01 \text{ sec}^{-1}$ (a) and $\dot{\varepsilon} = 10 \text{ sec}^{-1}$ (b).

ing during the deformation are absorbed by low-angle boundaries with growth of the strain at a relatively high temperature. As a result, the LAGB progressively transfer into HAGB [20]. After compression, the ferrite acquires a great number of equiaxed grains as a result of the interaction between the strain-induced dislocations and the low-angle grain boundaries. This phenomenon is usually called continuous dynamic recrystallization (CDR) [21]. However, at a higher strain rate ($\dot{\varepsilon} = 30 \text{ sec}^{-1}$) the process of CDR caused by the transformation of LADB into HAGB in the ferrite develops with a lower intensity due to the lower strain partitioning (Fig. 3e and f). This becomes obvious if we compare the structures of the steel deformed at $\dot{\varepsilon} = 0.01$ and 30 sec^{-1} . Under the deformation with strain up to 0.8 and $\dot{\varepsilon} = 0.01 \text{ sec}^{-1}$, the fraction of HAGB in the ferrite amounts to about 62%; at $\dot{\varepsilon} = 30 \text{ sec}^{-1}$ it is only about 28%, which means that the CDR in the ferrite develops much less. At the same time, dynamic recrystallization grains are still absent on the deformed boundaries of the austenite grains.

Thus, we may conclude that at a constant deformation temperature the degree of the dynamic softening of the ferrite decreases with increase of the strain rate. Since the strain at the early deformation stages is mainly controlled by the ferritic (soft) phase, the dislocation density in the austenite after the true strain of up to 0.4 remains low (Fig. 4a). When the strain rate is increased, the dislocations in the austenite become entangled and their density increases considerably (Fig. 4b). At a higher strain rate, the lower strain partitioning between the phases not only weakens the CDR in the ferrite, but also raises somewhat the strain hardening of the austenite. This is obviously the main reason behind the interruption of the uniform lowering of the activation energy in the intermediate deformation stage (Fig. 2c – e).

Increase of the temperature to 1423 K at a high strain rate (30 sec^{-1}) causes growth of the fraction of HAGB in the ferrite to 35% after the deformation with $\varepsilon = 0.8$ (Fig. 5a and b), which is much higher than at 1323 K (Fig. 3e and f). On the contrary, the lowering of the deformation temperature

to 1223 K at $\varepsilon = 0.8$ reduces the fraction of HAGB in the ferrite to 15% (Fig. 5c and d), which indicates a favorable effect of elevation of the temperature on the development of CDR in the ferrite. Moreover, the results of the quantitative metallographic analysis with the help of the Image Pro-Plus software show that when the deformation temperature is decreased in the range of 1473 – 1223 K, the content of austenite in the structure increases from about 35 vol.% to about 50 vol.% (Fig. 5c), which agrees with the data of [13, 27]. The higher austenite content (Fig. 5c) and the elevated deformation energy [19] at lower temperatures promote nucleation and growth of some fine austenite grains at the places with high energy, such as grain boundaries, which yields a necklace-type structure in the austenite. This process is termed discontinuous dynamic recrystallization (DDR) and is frequent in materials with low stacking fault energy including γ -Fe and copper [23, 24]. Consequently, the lowering of the deformation temperature (without changing the strain rate) reduces the CDR in the ferrite and activates the DDR in the austenite.

Strain maps. As a rule, the strain rate and the temperature of hot deformation are the main factors affecting the plastic flow behavior and the microstructure of the material. The choice of the process parameters is the most important aspect of hot deformation of steels and alloys. Maps of the deformation mechanisms based on dynamic modeling make it possible to develop recommendations for selection of the required hot treatment parameters for the material.

The deformation maps plotted from the maps of energy dissipation reflect the deformation mechanisms implemented in the material at various parameters. The constitutive equations can characterize the response of the metal in terms its effective flow stress σ . The following power equation is used the most frequently [25]:

$$\sigma = K \dot{\varepsilon}^m \Big|_{T, M}, \quad (3)$$

where M is a coefficient dependent on the history of fabrication of the initial sample, T is the Kelvin temperature, K and

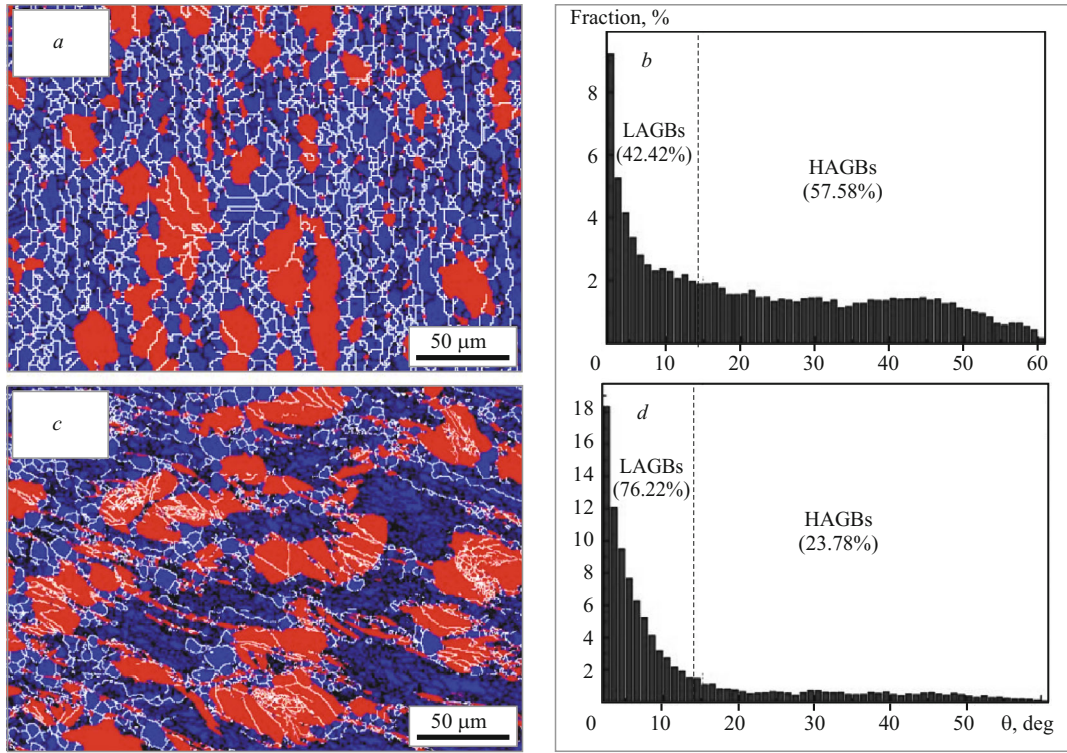


Fig. 5. EBSD maps of misorientations of ferrite and austenite grains and the respective histograms of distribution of grain boundaries in ferrite with respect to misorientation angles for different deformation parameters of steel DSS 2205 (part II): *a, b*) $T = 1423$ K, $\dot{\varepsilon} = 30 \text{ sec}^{-1}$, $\varepsilon = 0.8$; *c, d*) $T = 1223$ K, $\dot{\varepsilon} = 30 \text{ sec}^{-1}$, $\varepsilon = 0.8$.

m are constants. Dynamic simulation shows that when the material is deformed, the absorbed energy is mainly spent on plastic flow and transformation of the microstructure [25]. Accordingly, the absorbed energy is determined from the relation

$$P = \sigma \dot{\varepsilon} = G + J = \int_0^{\dot{\varepsilon}} \sigma d\dot{\varepsilon} + \int_0^{\sigma} \dot{\varepsilon} d\sigma, \quad (4)$$

where J and G are the energies spent on the transformation of the structure and on the straining, respectively, and P is the total energy absorbed by the material. Thus, the proportion of J and G determines the sensitivity of the stress (m) to the strain rate, i.e.,

$$\frac{dJ}{dG} = \frac{\dot{\varepsilon} d\sigma}{\sigma d\dot{\varepsilon}} = \frac{d \ln \sigma}{d \ln \dot{\varepsilon}} = m. \quad (5)$$

Consequently,

$$J = \frac{m}{m+1} \dot{\varepsilon} \sigma, \quad (6)$$

In order to determine the energy spent of the transformation of the structure of the material, the dissipated energy

may be described in terms of parameter η using the equation

$$\eta = \frac{J}{J_{\max}} = \frac{\sigma \dot{\varepsilon} m / (m+1)}{\sigma \dot{\varepsilon} / 2} = \frac{2m}{m+1}. \quad (7)$$

A large value of η in the energy dissipation maps corresponds to a higher energy spent on the change in the microstructure, which corresponds to active development of the process of softening. Consequently, the best process parameters of hot deformation of steels and alloys correspond to maximum values of η . However, instability of plastic flow of the metal may sometimes raise the value of parameter η in the range of instability. To make a correct choice of the parameters of hot deformation, we should also plot the maps of instability of the process and use them for determining the corresponding Prasad criterion [26]

$$\xi(\dot{\varepsilon}) = \frac{\partial \ln [m / (m+1)]}{\partial \ln \dot{\varepsilon}} + m. \quad (8)$$

The process parameters at which the variation of the entropy in hot deformation is less than the strain rate in the system (when $\xi < 0$) match the range of instability of plastic flow of the metal.

Relation between energy dissipation and $\ln Z$. With allowance for the considerations presented, we give in Fig. 6

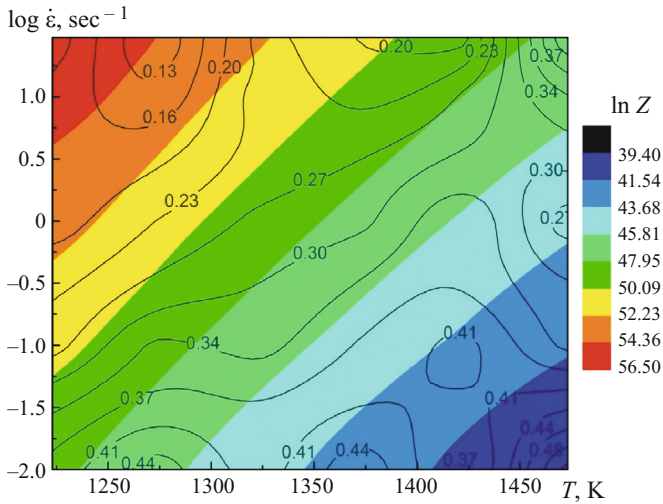


Fig. 6. Energy dissipation maps (the values of parameter η are given at the curves) of steel DSS 2205 at $\varepsilon = 0.5$ with superimposed map of instability of $\ln Z$.

the map of energy dissipation at true strain 0.5 with superimposed map of instability of $\ln Z$. The data show that the dissipation of energy varies with the variation of $\ln Z$, and the parameter η increases with decrease in $\ln Z$. Consequently, the decrease of Z corresponds to the decrease of the strain rate and increase of the deformation temperature, which intensifies the migration of grain boundaries and dislocations and activates dynamic retrogression and dynamic recrystallization in the steel, especially in ferrite. These processes lower the stress concentration on grain boundaries, and the proportion of the energy spent on the structural changes is increased. On the contrary, when the compression is accompanied by an increase of Z (Figs. 3e and 5d), the process of CDR in ferrite is suppressed considerably, which leads to a considerable growth of the proportion of the energy spent on plastic flow and decrease of the energy spent on structural transformations.

Maps of deformation mechanisms. Figure 7 presents the deformation maps of steel DSS 2205 plotted by imposition of instability maps onto maps of energy dissipation at true strains $\varepsilon = 0.2, 0.4, 0.5$ and 0.8 . It can be seen that the domains with negative values of ξ change with growth of the strain. It follows from Fig. 7a that instability of plastic deformation appears at a relatively high strain rate and has two zones. Zone 1 corresponds to the deformation temperatures of 1260–1300 K when the logarithm of the strain rate varies within 0.75–1.47. The ranges of the strain rate logarithms 0.45–1.47 and of the deformation temperatures 1360–1440 K correspond to zone 2. However, when the strain grows, the domains of instability of plastic flow change much (Fig. 7b–d), i.e., zone 2 becomes narrower and disappears virtually fully at a true strain of 0.8; on the contrary, zone 1 grows.

We have mentioned that at the start of compression deformation is implemented almost completely in the soft ferrite phase [10]. At higher strain rates, the annihilation of dislocations is suppressed somewhat due to the shortage of time as compared to the high strain rates. This results in intense stress concentration on grain boundaries and in a relatively low value of ξ . However, when the strain rate is increased, the behavior of the steel with the temperature changes. In compression at a relatively high temperature (1423 K, Fig. 5a and b), the CDR in ferrite is activated with growth of the strain, which lowers effectively the stress concentration in the alloy and improves the deformability of the material. If the deformation temperature is decreased to 1323 K, the CDR in the ferrite becomes much weaker, and this affects unfavorably the stability of plastic flow of the metal under hot deformation.

However, with further decrease of the temperature to 1223 K (Fig. 5c and d) the compressibility of the steel improves again. This is explainable by the positive influence of austenite on the process of plastic flow of the metal at relatively low temperatures and high strain rates, because the content of austenite in the structure of the duplex steel increases and the strain is partitioned. At $\varepsilon = 0.8$ and $T = 1223$ K (Fig. 5c and d) the activated process is DDR in the austenite; together with the CDR in the ferrite this makes it possible to avoid the appearance of negative ξ and provides a high hot compressive deformability of the metal.

It can be inferred that instability of plastic flow arises in steel DSS 2205 primarily in the early deformation stages at high strain rates. At 1360–1440 K, plastic flow chiefly occurs in ferrite due to its high content and strain adaptability. At a higher strain the ferrite undergoes CDR, the flow stability in the metal grows, and so does the value of ξ . Lowering of the deformation temperature and elevation of the strain rate weaken the process of CDR in ferrite even at a high strain. As a result, the area of zone 1 in the deformation map increases instead of being decreased (Fig. 7). Figure 8 presents a typical microcrack formed in the structure of steel DSS 2205 during hot compression at 1323 K at a rate of 10 sec^{-1} , which agrees with the data of the deformations maps in Fig. 7. It can be seen in Fig. 8 that the crack has nucleated on phase boundaries and propagated over the interphase in the soft ferrite.

CONCLUSIONS

We have analyzed the mechanism of hot deformation of duplex stainless steel DSS 2205 by studying the interrelation between the hot deformation parameters and the evolution of the microstructure. The mechanisms of plastic flow in the ferrite and in the austenite of the duplex steel differed and obeyed the following laws.

1. The flow stress in the metal increased with increase of the strain rate and lowering of the deformation temperature. The stress-strain curves for the process of hot compression at

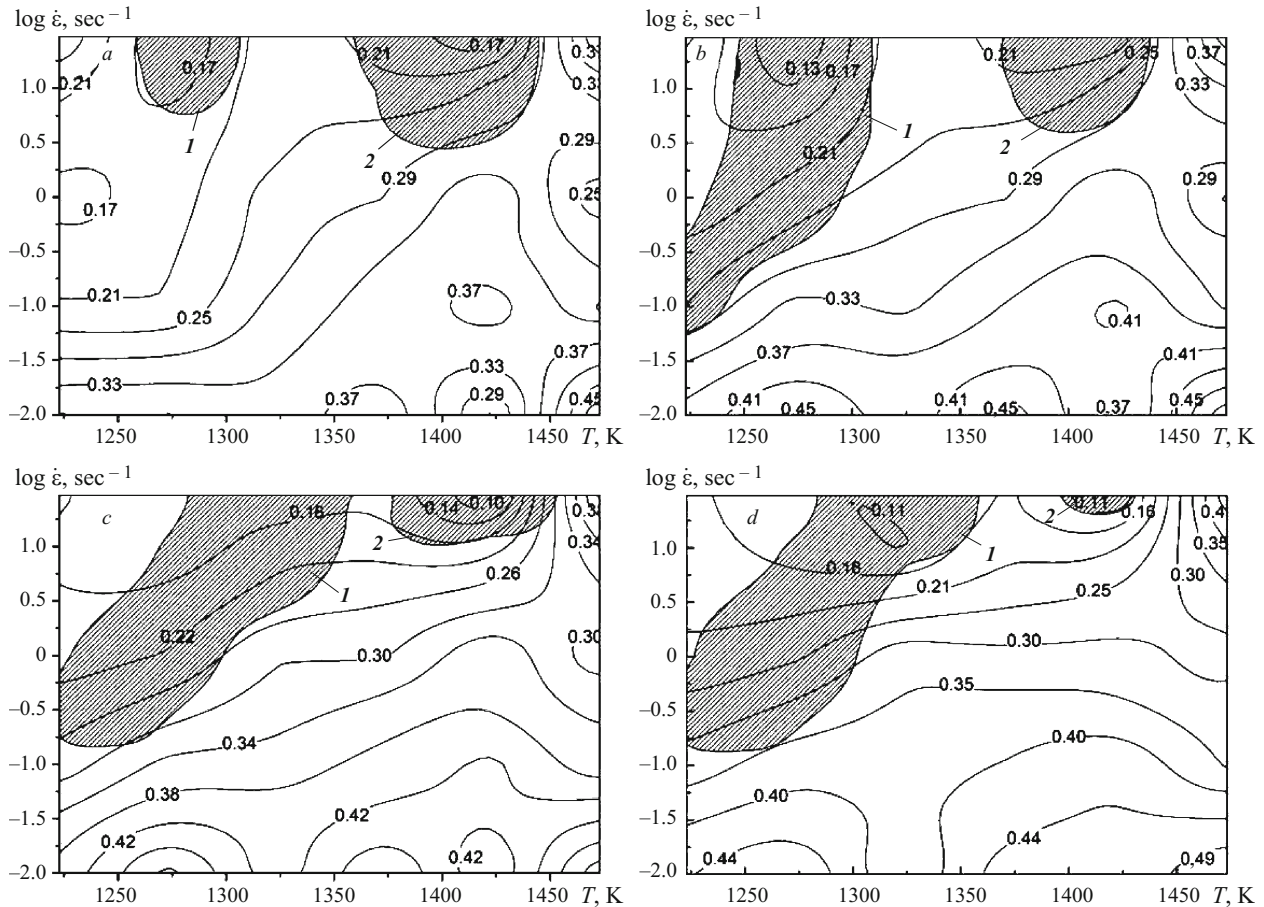


Fig. 7. Deformation maps of steel DSS 2205 plotted by imposition of instability maps onto maps of energy dissipation at different true strains: *a*) $\varepsilon = 0.2$; *b*) $\varepsilon = 0.4$; *c*) $\varepsilon = 0.5$; *d*) $\varepsilon = 0.8$; the values of parameter η are given at the curves; 1 and 2) the zones of unsteady deformation are hatched.

a rate of $1 - 30 \text{ sec}^{-1}$ at 1373 K had a wavy pattern and a region of softening after the attainment of maximum stress. At

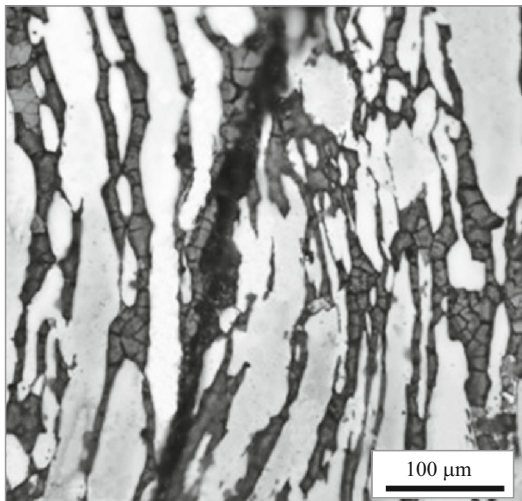


Fig. 8. Microcrack in the structure of steel DSS 2205 after deformation at strain rate 10 sec^{-1} at 1323 K .

strain rates $0.01 - 0.1 \text{ sec}^{-1}$, the curves varied smoothly and the softening region was almost absent.

2. The activation energy Q of hot deformation decreased with growth of the true strain ε from 0.10 to 0.75. However, in the range of $\varepsilon = 0.3 - 0.6$ the intensity of the continuous dynamic recrystallization in the ferrite was reduced, and the influence of the austenite of the plastic flow behavior grew, which caused softening of the structure of the metal under hot deformation and stopped the lowering of Q .

3. During compression, the degree of energy dissipation increased with lowering of $\ln Z$. In the initial stage of the deformation, the instability of the plastic flow had two zones. With growth of the strain, the area of the first zone increased and that of the second zone narrowed gradually and virtually disappeared after the true strain of 0.8.

4. Decrease of the deformation temperature and increase of the strain rate were accompanied by suppression of the continuous dynamic recrystallization in the ferrite, weak dynamic softening of the two phases, and formation of microcracks. The microcracks nucleated on phase boundaries and propagated over them into the soft phase, i.e., ferrite.

This research was funded by the National Natural Science Foundation of China, grant number 52005304; the Natural Science Foundation of the Shandong Province, grant number ZR2019BEE034; the National Natural Science Foundation of China, grant number 52175342; the Natural Science Foundation of the Shandong Province, grant number ZR2021ME129; the Taiyuan University of Science and Technology Scientific Research Initial Funding (20202039).

REFERENCES

1. C. M. Garzon and A. P. Tschiptschin, "EBSD texture analyses of a high temperature gas nitride duplex stainless steel," *Mater. Sci. Eng. A*, **441**(1–2), 230–238 (2006).
2. J. M. Cabrera, A. Mateo, L. Lanes, et al., "Hot deformation of duplex stainless steels," *J. Mater. Process. Technol.*, **143–144**, 321–325 (2003).
3. A. L. Filho, J. M. D. A. Rollo, R. V. Silva, and G. Martinez, "Alternative process to manufacture austenitic(ferritic stainless steel wires)," *Mater. Lett.*, **59**(10), 1192–1194 (2005).
4. E. Evangelista, H. J. McQueen, M. Niewczas, and M. Cabibbo, "Hot workability of 2304 and 2205 duplex stainless steels," *Can. Met. Quart.*, **43**, 39–353 (2004).
5. A. Momeni, S. M. Abbasi, and A. Shokuhfar, "Hot compression behavior of as-cast precipitation-hardening stainless steel," *J. Iron Steel Res. Int.*, **14**, 66–70 (2014).
6. O. A. Zambrano, J. Valdés, Y. Aguilar, et al., "Hot deformation of a Fe–Mn–Al–C steel susceptible of *k*-carbide precipitation," *Mater. Sci. Eng. A*, **689**, 269–285 (2017).
7. Q. A. Gao, H. L. Zhang, H. J. Li, and C. C. Jiang, "Hot deformation of alumina-forming austenitic steel: EBSD study and flow behavior," *J. Mater. Sci.*, **54**(11), 8760–8777 (2017).
8. N. D. Ryan and H. J. McQueen, "Flow stress, dynamic restoration, strain hardening and ductility in hot working of 316 steel," *J. Mater. Process. Technol.*, **21**(2), 177–199 (1990).
9. A. I. Rudskoy, A. A. Kononov, S. Yu. Kondrat'ev, and M. A. Matveev, "Texture formation in hot rolling of electrical anisotropic steel," *Met. Sci. Heat Treat.*, **60**(11–12), 689–694 (2019).
10. O. Balancin, W. A. M. Hoffmann, and J. J. Jonas, "Influence of microstructure on the flow behavior of duplex stainless steels at high temperatures," *Metall. Mater. Trans. A*, **31A**, 1353–1364 (2000).
11. A. Iza-Mendia, A. Pinol-Juez, J. J. Urcola, and I. Gutierrez, "Microstructural and mechanical behavior of a duplex stainless steel under hot working conditions," *Metall. Mater. Trans. A*, **29A**, 2975–2986 (1998).
12. Y. Y. Liu, H. T. Yan, X. N. Wang, and M. Yan, "Effect of hot deformation mode on the microstructure evolution of lean duplex stainless steel 2101," *Mater. Sci. Eng. A*, **575**, 41–47 (2013).
13. G. W. Fan, J. Liu, P. D. Han, and G. J. Qiao, "Hot ductility and microstructure in casted 2205 duplex stainless steels," *Mater. Sci. Eng. A*, **515**(1–2), 108–112 (2009).
14. Y. Wang, Q. L. Pan, Y. F. Song, et al., "Hot deformation and processing maps of X-t50 nickel-based superalloy," *Mater. Des.*, **51**, 154–160 (2013).
15. Y. H. Liu, Y. Q. Ning, Z. K. Yao et al., "Effect of true strains on processing map for isothermal compression of Ni–20.0Cr–2.5Ti–1.5Nb–1.0Al Ni-base superalloy," *J. Alloy Compd.*, **612**, 56–63 (2014).
16. C. Zener and J. H. Hollomon, "Effect of strain rate upon plastic flow of steel," *J. Appl. Phys.*, **15**(1), 22–32 (1944).
17. C. M. Sellars and W. J. McG, "Hot workability," *Int. Metal.*, **17**, 1–24 (1972).
18. Y. H. Yang and B. Yan, "The microstructure and flow behavior of 2205 duplex stainless steels during high temperature compression deformation," *Mater. Sci. Eng. A*, **579**, 194–201 (2013).
19. A. Momeni, K. Dehghani, and M. C. Poletti, "Law of mixture used to model the flow behavior of a duplex stainless steel at high temperatures," *Mater. Chem. Phys.*, **139**(2–3), 747–755 (2013).
20. B. Eghbali, A. Abdollah-Zadeh, H. Beladi, and P. D. Hodgson, "Characterization on ferrite microstructure evolution during large strain warm torsion testing of plain low carbon steel," *Mater. Sci. Eng. A*, **435–436**, 499–503 (2006).
21. J. C. Tan and M. J. Tan, "Dynamic continuous recrystallization characteristics in two stage deformation of Mg–3Al–1Zn alloy sheet," *Mater. Sci. Eng. A*, **339**, 124–132 (2003).
22. M. Martins and L. C. Casteletti, "Heat treatment temperature influence on ASTM A890 GR 6A super duplex stainless steel microstructure," *Mater. Charact.*, **55**(3), 225–233 (2005).
23. H. Hallberg, B. Svendsen, T. Kayser, and M. Ristinmaa, "Microstructure evolution during dynamic discontinuous recrystallization in particle-containing Cu," *Comp. Mater. Sci.*, **84**, 327–338 (2014).
24. D. G. Cram, X. Y. Fang, H. S. Zurob, et al., "The effect of solute on discontinuous dynamic recrystallization," *Acta Mater.*, **60**(18), 6390–6404 (2012).
25. P. Zhang, C. Hu, C. G. Ding, et al., "Plastic deformation behavior and processing maps of a Ni-based superalloy," *Mater. Des.*, **65**, 575–584 (2015).
26. Y. V. R. K. Prasad, H. L. Gegel, S. M. Doraivelu, et al., "Modeling of dynamic material behavior in hot deformation: Forging of Ti-6242," *Metall. Mater. Trans. A*, **5A**, 1883–1892 (1984).